Published in final edited form as:
Science. 2013 November 1; 342(6158): 1238406. doi:10.1126/science.1238406.

Cortical High-Density Counterstream Architectures

Nikola T. Markov[1,2,3], **Mária Ercsey-Ravasz**[4], **David C. Van Essen**[5], **Kenneth Knoblauch**[#1,2], **Zoltán Toroczkai**[#6,7,†], and **Henry Kennedy**[#1,2,†]

[1]Stem cell and Brain Research Institute, INSERM U846, 18 Avenue Doyen Lépine, 69500 Bron, France

[2]Université de Lyon, Université Lyon I, 69003 Lyon, France

[3]Yale University, Department of Neurobiology, New Haven, CT 06520, USA

[4]Faculty of Physics, Babeş-Bolyai University, Cluj-Napoca, 400084 Romania

[5]Department of Anatomy and Neurobiology, Washington University School of Medicine, St. Louis, MO 63110-1093, USA

[6]Department of Physics and Interdisciplinary Center for Network Science and Applications, University of Notre Dame, Notre Dame, IN 46556, USA

[7]Max Planck Institute for the Physics of Complex Systems, 01187 Dresden, Germany

[#] These authors contributed equally to this work.

Abstract

Small-world networks provide an appealing description of cortical architecture owing to their capacity for integration and segregation combined with an economy of connectivity. Previous reports of low-density interareal graphs and apparent small-world properties are challenged by data that reveal high-density cortical graphs in which economy of connections is achieved by weight heterogeneity and distance-weight correlations. These properties define a model that predicts many binary and weighted features of the cortical network including a core-periphery, a typical feature of self-organizing information processing systems. Feedback and feedforward pathways between areas exhibit a dual counterstream organization, and their integration into local circuits constrains cortical computation. Here, we propose a bow-tie representation of interareal architecture derived from the hierarchical laminar weights of pathways between the high-efficiency dense core and periphery.

Because the concepts of localization of function and parcellation into cortical areas are closely intertwined, elucidating the global pattern of areal interactions is central to understanding higher brain functions (1–5). Cerebral cortex in the macaque monkey is sub-divided into a mosaic of ~100 cortical areas, each displaying characteristic features, including cytoarchitecture (6). Each area has a characteristic connectivity profile thought to contribute to determining its functional properties (1, 7, 8). Here, we review how interareal connectivity at the single-cell level (9), revealed by quantitative anatomical tract tracing, is relevant to our understanding of large-scale cortical networks and their hierarchical organization (8, 10–13).

The circuitry of cerebral cortex is dominated by local (within-area) connections, and interareal connections constitute only about 20% of total cortical connectivity. Hence, the dozens of long-distance projections to areas beyond the immediate neighboring areas

[†]Corresponding author. henry.kennedy@inserm.fr (H.K.); toro@nd.edu (Z.T.).

account for ~ 5% (10). Local networks conform in many ways to a canonical microcircuit that spans all cortical layers (14, 15) and includes recurrent excitation presumed to shape and amplify the sparse input from subcortical and distant cortical sources (16).

Felleman and Van Essen (FVE) showed that interareal connectivity obeys hierarchical constraints rooted in the strong anatomical regularities of feedforward and feedback pathways (17). In this way, multiple distributed cortical hierarchies form a large-scale model of the cortex (17) that reflects the laminar integration of interareal connectivity into local circuits (18) and is relevant to sensory (17, 19, 20), motor (21, 22), and cognitive (23–27) systems. The structural features of interareal interactions may provide important insights into the observed dynamics of large-scale interareal networks controlling information flow through the cortex (1, 28, 29).

Density and Small-World Architectures

Graph theory provides a powerful framework for investigating complex networks such as those found in the brain. Many insights into the functional processes supported by such networks have been gleaned from analysis at the binary level (i.e., connections present or absent; see Glossary for definitions) (30). One important class of models that has received much attention is that of small-world (SW) networks, distinguished by high clustering coupled with a short average path length (also called characteristic path length) across the graph (31). The relevance of the SW property to understanding the cortex comes from its proposed capacity to optimize essential cortical features, including functional integration and segregation (32, 33).

Several studies based on collations of published anatomical tract tracing data (34–38) concluded that the cortical interareal network conforms to the SW network model of Watts and Strogatz (31). According to this hypothesis, efficient signal propagation through cortical circuits benefits from a modest number of shortcuts connecting different communities across the cortical graph.

The SW hypothesis for interareal connectivity has been challenged by recent studies that used a consistent and optimized methodology to establish a quantitative data-base of macaque interareal connectivity (8, 11). We segmented the cortical sheet into 91 cortical areas and quantitatively analyzed the incoming connections to a subset of 29 areas chosen to represent five major regions of the cortex. By using similar procedures and identical area definitions across brains, this effort set out to overcome the limitations inherent in collated datasets that combine results across many anatomical studies (39). These limitations arise from the diversity of procedures used among different anatomical studies, including cross-study differences in parcellation schemes, extent of cortex examined, tracer sensitivity, criteria for accepting the presence or absence of a connection, and the spatial resolution of the analysis.

Injections of retrograde tracers in the 29 areas revealed 36% more connections than previously reported (8, 10). These so-called new-found projections (NFPs) were presumably missed by earlier studies for several reasons, including that they link widely separated areas (long-distance connections) and tend to be sparse, therefore requiring high resolution obtained by optimized sampling frequency for their detection (40, 41). Notably, repeat injections in selected areas and statistical modeling of the variability of projection magnitude demonstrated well-defined weighted connectivity profiles for each area and indicated high consistency for pathways of sufficient strength (8, 10). Inclusion of the NFPs considerably increases the cortical network density (i.e., the number of binary connections that exist relative to the total number of connections possible) (42). The density of the full

interareal network (FIN), represented by the graph (or matrix) $\boldsymbol{G}_{91\times91}$, remains unknown. However, a dominating set analysis of the currently known interareal network represented as the $\boldsymbol{G}_{29\times91}$ subgraph of the FIN predicts that the FIN is itself a densely connected network (8).

The $\boldsymbol{G}_{29\times29}$ interareal subgraph, formed among the injected (target) nodes, is edge-complete (see Glossary), and it has a link density of 66% (i.e., two-thirds of connections that can exist do exist) (8). The $\boldsymbol{G}_{29\times29}$ is denser than any subgraph used in previous studies of the cortical network. Figure 1A displays the differences in density and average path length of various published subgraphs that have been used to investigate the large-scale properties of the cortex. FVE analyzed several hundred publications and reported on 32 visual areas and 305 pathways, for a graph density of 32% (17). In their meta-analysis, many pathways were identified as untested (i.e., the subgraph was edge-incomplete); they predicted a density of 45% if the unknown connections were to be tested. Three subsequent studies added collated data to the FVE data set, thus generating subgraphs of 47 areas $\boldsymbol{G}_{47\times47}$ (34), 71 areas $\boldsymbol{G}_{71\times71}$ (43), and 179 areas $\boldsymbol{G}_{179\times179}$ (44), respectively. The resulting subgraphs were also edge-incomplete, but untested connections were assigned a “nonconnection” status, leading to low density estimates ranging from 5 to 25%. Jouve *et al*. updated the FVE data set with additional connections reported during the 7-year interval between the two studies, yielding an observed density of 37% (45). They used an inference algorithm based on second-order connection regularities and arrived at a density prediction of 58% for visual cortex.

The aggregate evidence suggesting high density of the FIN of the macaque neocortex led us to explore the implications for putative SW properties of the dense cortical graph. In contrast with *d*-dimensional regular lattices, where the characteristic path length L grows as a power-law $L \propto n^{1/d}$ with the number of nodes n, in a SW network path length growth is logarithmic with the number of nodes and hence much slower, i.e., as $L \propto \frac{\ln n}{\ln k}$, where k is the average degree in the network (31, 46). Figure 1B examines the effect of density on a hypothetical 1000-node ring lattice network on the interval over which the SW phenomenon of high clustering and short path length exists. The reduction in average path length and increase in clustering of a lattice by random rewiring of connections is density dependent. At densities below about 42%, even limited rewiring substantially decreases average path length while maintaining high clustering, thereby providing shortcuts characteristic of a SW architecture. By contrast, at high densities rewiring barely affects path length, because density alone determines this feature, independently of the more detailed structure of the network. Figure 1C shows the SW coefficient as a function of rewiring probability for regular networks (lattices) with increasing density [defined as in (31)]. These results indicate that the density predicted by FVE (45%) and that reported by Markov *et al*. (8) would reject the hypothesis of the large-scale interareal cortical network being a Watts-Strogatz–type SW network.

The $\boldsymbol{G}_{29\times29}$ matrix discussed here has a density of 66% and includes pathways with few labeled neurons. As we have argued elsewhere, weak pathways could fulfill diverse roles (8, 10, 11, 13, 39), and given that injections involve only a fraction of a target area, we do not capture the full complement of neurons for each weak pathway. Thresholding would reduce the range of weights that we report. For example, eliminating pathways with, on average, fewer than 10 neurons per tracer injection would reduce the graph density from 66 to 53%, and the range of connection weights (8) from five to four orders of magnitude. At 53%, our conclusions concerning the SW would not change. However, 37% of the pathways that would be eliminated by this thresholding have been reported in earlier publications. Further, these conservative steps would ignore the possibility that much larger injections coupled with higher sampling could potentially reveal larger cell numbers, thereby increasing the

range of connection weights, numbers of areas connected, and the graph density with respect to the values reported here.

At graph densities approaching 100%, the point when all pairs of nodes are interconnected, the variability within the graph's structure approaches zero. Hence, at the high density found in the $\boldsymbol{G}_{29\times29}$ matrix, little binary specificity might be expected. However, because the probability of connections drops steeply with distance, the subset of long-distance connections can show binary specificity, as we demonstrate in the next section.

Binary Specificity in the High-Density Cortical Graph

Figure 2A shows the $\boldsymbol{G}_{29\times29}$ matrix with the NFPs indicated in red and organized so that target areas are associated with one of the five regions of the cortex (occipital, temporal, parietal, frontal, and pre-frontal; see Fig. 2D). Earlier anatomical studies suggested that cortical areas are preferentially connected to physically nearby areas in the region in which they are located, whereas the additional NFPs mainly interconnect area pairs located in different regions (8). Because regionally related areas tend to have similar connectivity patterns, this raises the question of whether the NFPs are perhaps important because they connect areas having dissimilar connectivity patterns. Using a similarity index (see Fig. 2B), we measured the degree to which two areas receive (or avoid receiving) input from common sources (in-link similarity) (11). This confirmed that within-region similarity was high; between-region similarity was lower and, notably, declined with increasing distance between regions (Fig. 2B). The observation that NFPs tend to interconnect distant areas with low similarity provides one indication of their specificity.

Additional evidence for the NFP-related specificity comes from a dominating set analysis, a graph theoretical method that quantifies the extent to which connections are gathered (“dominated”) by a small set of nodes (8, 11). In the case of directed networks, in-link and out-link domination are specified separately. Because with retrograde tracers all the in-links are revealed for an injected target area (but not the out-links), we focused on in-link domination (8, 11). A subset of nodes is said to be fully in-link dominating if all nodes of the graph each project to at least one edge into this subset. There can be several fully dominating sets of nodes (areas); a minimum fully dominating set (MDS) is the smallest such set. The smaller the MDS, the more concentrated the input, indicating the increased role that this set plays in the network. A more refined measure is given by encoding the percentage of all nodes that project into a group of given target areas (8, 11) (thus 100% corresponds to full domination). The histogram of this fraction over all possible groups of a given size (e.g., all combinations of two or more targets) gives an overall picture of domination; see fig. S3, A and B, in (11) for the $\boldsymbol{G}_{29\times91}$ network. In this case, the low value of 2 for the MDS along with the high domination percentage of many small groups of target areas indicates that the FIN must also be a dense network [see (8) for more details]. Comparing these histograms with and without the NFPs included shows that the NFPs play a key role in the statistics of the inputs to area groups, as their removal appreciably reduces domination for all sets, and the MDS size jumps from 2 to 5 (11).

Besides suggesting a key role for the NFPs, the dominating set analysis confirms the high density of the cortical graph (11). However, this density is not homogeneously distributed. The percentage of areas projecting to a target area is 99% for areas within 10 mm, 85% between 10 and 20 mm, 50 to 60% between 20 and 40 mm, and below 40% at 40 mm or greater. Examination of the cortical areas projecting to a target region shows that a modest number of areas outside that region project to all of the injected areas included in the target region (11) (Fig. 2D). Thus each target region has a set of common input areas, which constitute a connectivity signature of the target region (1, 7, 11). The number of common

input areas to a region is substantially larger when NFPs are included (red versus blue in Fig. 2D). Comparisons with randomly permuted networks indicate that the increase in the number of common inputs after inclusion of NFPs significantly exceeds that which would occur from an increase in density by the addition of an equivalent number of random connections (11). Further, the specificity of the long-distance connections and hence of the NFP is indicated by the fact that the density of the interregional edge-complete graphs is considerably lower than for those formed by intraregional connections (Fig. 2C). Note, that the specificity of the NFP connectivity is the same as for all long-distance connections, including those already known (11).

The impact of the interareal pathways on the physiology of the target areas is constrained by the laminar origins of the parent neurons of the pathway and the cortical layers targeted by their synaptic terminals. These laminar constraints on interareal pathways contribute to determining cortical hierarchies (17), which we address in the next section.

Hierarchical Organization

More than 70% of all the projections to a given locus on the cortical sheet arise from within 1.5 to 2.5 mm, so that cortical connectivity is dominated by short-distance (10), local connections that conform to a canonical microcircuit optimized to amplify and shape weaker long-distance cortical inputs (Fig. 3A) (16). Therefore, when considering long-distance interareal pathways, it is important to consider not only the strength and the specificity of the connections, but also their pronounced laminar asymmetry determined by the direction of the connection. Hence, feedforward (FF) pathways (mostly directed rostrally) originate principally from supragranular layers and terminate in layer 4 in higher areas (47–49), whereas feedback (FB) pathways (mostly directed caudally) originate mainly from infragranular layers in higher areas and avoid layer 4 in lower areas (47, 49–51). Pairwise comparison of the connections has been used to reveal cortical hierarchies (17, 52). While the FVE model is indeterminate (53), it can be partially resolved by using a continuous scale such as hierarchical distance based on the fraction of supragranular layer neurons (SLNs) (Fig. 3B) (54–56). The SLN index quantifies an order relation between areas as defined by their laminar profiles of connectivity and thereby allows estimation of the hierarchical distance separating them (57). Further analysis shows that connections between neighboring areas have the highest weight, defined as the fraction of labeled neurons (FLN) (10, 58), whereas long-distance FF and FB connections have lower weights (Fig. 3, B and C).

Interest in the hierarchical organization of the cortex is fueled by evidence that FF and FB processes are distinct physiologically. A useful, albeit oversimplified characterization is that FF connections are “driving” and FB connections are “modulatory” (59–63). Further, FF and FB pathways engage different glutamate receptor subtypes (64). If the two polarities indeed have relatively distinct roles, one might predict that any given neuron would contribute to only one type of pathway, rather than supplying axons to both. This has been tested by injecting two distinguishable retrograde tracers in higher and lower cortical areas and examining the intermediate areas for double-labeled neurons (i.e., neurons with a bifurcating axon directed at both pathways). The results showed that the FF and FB neurons in the intermediate areas were virtually all single-labeled, which is striking given the commonality of axonal bifurcation (57, 65). Not only do FF and FB constitute distinct populations, but they also form two segregated streams, consistent with earlier observations (47, 66, 67). The supra- and the infragranular layers each have a counterstream organization, most pronounced in the supragranular layers (Fig. 3D) (12, 68). Further, the supragranular counterstream showed a point-to-point (i.e., topographical) precise connectivity in both FF and FB directions, whereas the infragranular counterstream has a more diffuse topography showing high divergence and convergence in both directions (12). Hence, contrary to

previous assertions, topographic precision distinguishes supragranular layer from infragranular connections and not FB versus FF pathways (12).

The integration of interareal connections into the canonical microcircuit of a target area presumably determines how top-down and bottom-up streams affect processing within the target area (18). The concept of hierarchical processing has influenced theories of cortical computation, predictive coding, and emerging concepts of inference in cortical function (18, 69, 70). Recent progress in elucidating interareal communication includes the demonstration of gamma-band phase coherence in the supragranular and beta-band coherence in the infragranular layers (71, 72). These differences in coherence reflect differences in interareal synchronization (73–76), which are thought to facilitate effective communication (74, 77). Recently beta-gamma asymmetries have been shown to correlate with the aforementioned SLN fraction, suggesting a match between anatomically and functionally defined hierarchies (18). The SLN analysis revealed infrequent, but potentially important, departures from the reciprocity of FF and FB projections. For instance, instead of FF being invariably reciprocated by FB, a few FF pathways are reciprocated by a FF, thereby forming a strong loop (54, 78, 79), which is illustrated in Fig. 3E, where the FF projection of V4 to the frontal eye field (area 8L) is reciprocated by a FF and not a FB connection (12, 54). Given the evidence for different physiological roles of FF and FB pathways, such anti-hierarchical pathways may allow circulation of information up and down the cortical hierarchy entirely via FF pathways. The functional importance of these rare so-called strong loops (79) remains to be determined.

Rich-Club and Bow-Tie Structure

Previous studies based on sparse cortical networks have suggested an important structural heterogeneity in the cortex, where hub areas are statistically more interconnected than expected, forming a so-called rich club (80–82) or central core (44). Using methods adapted to high-density graphs (83), we have shown that the $\boldsymbol{G}_{29\times29}$ subgraph harbors 13 cliques (complete subgraphs in which all possible connections are present) of size 10. This results in a very high, 92% density core formed of 17 nodes in the edge-complete $\boldsymbol{G}_{29\times29}$ (13), a periphery of 12 nodes with a density of 49%, and a 54% density of connectivity between the periphery and core. Because additional injections cannot change the structure of the $\boldsymbol{G}_{29\times29}$ subgraph, this implies that the FIN also has a dense core (to which the core of $\boldsymbol{G}_{29\times29}$ must belong, being 92% dense), possibly larger than that of $\boldsymbol{G}_{29\times29}$. The core-periphery distinction is also supported by the average strength of connections, as the fraction of labeled neurons (FLN, see Glossary) between the core and periphery is on average weaker than within either the core or periphery (13).

Next, we present a method (see captions of Table 1 and Fig. 4) that uses both the FLN weights and the SLN fractions to reveal correlations among core and periphery links (Fig. 4A), thereby providing further information on the large-scale organization of the cortical network. In Fig. 4B, peripheral nodes are split into two groups (Table 1). In the left fan, the preponderant pathways are FF going from the periphery to the core reciprocated by FB from the core to the periphery. In the right fan, the preponderant pathways are FB going from the periphery to the core reciprocated by FF pathways from the core to the periphery (Fig. 4B). The preponderant pathways being FF from left to right and FB in the inverse direction also holds for the small number of direct links between the two fans (see Fig. 4B). The core includes areas in the frontal, prefrontal, and parietal regions [see Fig. 2D for region locations and (8) for area members of each region]. The predominant FF inputs from the left wing to the core areas may serve as feeders for the central core processing (consistent with the inclusion of primary sensory and motor areas in this left wing; see Fig. 4B), whereas the FB

pathway predominance from the right wing could correspond to a monitoring or coordinating role for the members of this group.

A Cortical Distance Rule as Cost-of-Wiring Principle: The EDR Model

The above observations suggest a general picture of the interareal network: It is a dense network, but with high binary specificity ensured by long-distance connections and characterized by the existence of a core-periphery structure organized into a bow tie via FF/FB pathways. The specificity of connections increases with projection distance and with decreasing connection weights. Is there a fundamental, biophysical principle–based model that can capture most of these properties with a minimal number of fitting parameters? The answer is yes, as discussed below.

A clue to the importance of weight-distance relations for understanding the properties of the cortical network comes from the observation that the FLN weights are highly heterogeneous, following a log-normal distribution varying over five orders of magnitude (8, 10) (Fig. 5A). The log-normal distribution may directly reflect the interplay between metabolic costs associated with projection lengths and a geometrical or spatial property of areal locations (13). Axonal projections out to a distance d through the white matter come at an energy (metabolic) cost, irrespective of the areas involved. This is suggested by the exponential decay of the number of labeled neurons as a function of projection distance d: $p(d) = c\exp(-\lambda d)$, corresponding to an exponential distance rule (EDR) (Fig. 5B). The spatial decay constant $\lambda = 0.188\ \mathrm{mm}^{-1}$ expresses the growth rate of the metabolic cost with distance. We therefore expect that the FLN between two areas separated by a distance d is determined to a first approximation by this cost, independently of areal identity. A relevant spatial property is expressed by the inset in Fig. 5B, showing that the fraction of area pairs separated by a distance d is well approximated by a truncated Gaussian. Hence, combining the EDR with the Gaussian distribution of interareal distances, one finds that the distribution of area pairs with a given FLN indeed obeys a log-normal distribution (13).

These observations suggest that the EDR, which is a global distance rule, acts as a principle for resource allocation via the probability factor determined by the space constant λ. To what extent is the cortical network determined by this principle? To address this question, we defined two random network models [see (13) for details], one based on the EDR and the other on a constant distance rule (CDR, where projection length bears uniform cost). We then compared the statistical properties of these two sets of networks to those of the observed $\boldsymbol{G}_{29\times 29}$ subgraph. Only the EDR model captures the binary statistical graph properties of $\boldsymbol{G}_{29\times 29}$ on all scales (from local to global), including motif distributions (84) and graph spectral properties. Most notably, the EDR but not the CDR generates graphs with a pronounced core-periphery structure, closely tracking the distribution of cliques in the $\boldsymbol{G}_{29\times 29}$ (Fig. 5C). This figure also demonstrates that the CDR model fails to produce cliques of size 8 and larger. This finding suggests that the existence of the dense core in the cortex reflects the cost-of-wiring principle expressed in the EDR.

Efficiency of Information Transfer

A simple measure of bandwidth for information transfer in complex networks can be defined via the average conductance between all source-target pairs in the network (85), called global efficiency, or (E_g). Conductance here is interpreted as in physics, by the inverse resistance of the directed path of minimal total path resistance through the network from the source node to the target node (see Box 1 for definitions of the quantities in terms of FLNs). The path resistance can be interpreted as the negative logarithm of the probability that activity in the source node will generate activity in the target node. Here, we equate

bandwidth with axon number as reflected by FLN. Thus, a sequence of edges having large FLN values (or "high bandwidth" edges) directed from source to target would form a path of low resistance (high conductance), providing a high-bandwidth pathway for information transmission. To obtain a graded measure of global efficiency within the structure of $\boldsymbol{G}_{29\times29}$ and to understand the role of weak projections, we computed E_g on the remaining network after the sequential removal of the weakest link (smallest FLN) and plotted it as function of the network density. Figure 5D shows that the global efficiency of the network does not change before 76% of the weakest links are removed, indicating the existence of a high global efficiency (high bandwidth) backbone formed by short-range paths (see Fig. 5, E and F). Indeed, the average length of the remaining edges at 24% remaining density is 16 mm compared to the 27-mm average length of the removed edges. This suggests that the cortical network is organized in such a manner as to be independent of the activity along the weak projections for high-bandwidth information transfer. We speculate that these long-range pathways, which we have shown to have a high binary specificity, may contribute to interareal synchronization between cooperating areas.

A more local notion of information transfer can be similarly defined (86), via the average conductance between all the pairs of nodes that are neighbors of a given node *i*, after the removal of node *i*, then averaging this quantity over all nodes *i* (see Box 1), called local efficiency, E_l. One can think of E_l as a measure of accessibility between the satellites of a town via routes that avoid the town. Figure 5D shows this quantity as a function of density (following the same weakest-link removal procedure as above). Intriguingly, local efficiency increases sharply with weak-link removal (or inactivity), compared to the global efficiency. The weak-link removal increases locality because the weak links are long-range. This tends to prune the interregional shortcuts and physiologically would be predicted to decrease interactions between diverse functional modalities, leading to a more localized structure of the remaining network. It eliminates those neighbors of a node to which it connects via weak links, thus disconnecting regions and modalities but preserving dense within-region connections. Accordingly, the paths linking the remaining neighbors of the node (avoiding that node) are all strong, having small path resistance (large conductance), and hence the measure of local efficiency becomes large. The redundancy of local strong paths [the complete triangle is the most abundant three-motif, formed by strong links as shown in figure 3B of (13)] guarantees that the number of edges on a path between two nodes is small, which further decreases the path resistance between the nodes and hence further increases the local efficiency.

These changes in local efficiency indicate flexibility of network modularity and long-distance functional interactions—for example, in response to changes in cognitive load (13, 87). This suggests that in the cortical network, local information processing is voluminous, and because of the redundancy of local high-conductance paths, it is much more efficient than global information processing, whose efficiency acts at a constant base line (Box 1). Notably, the organization of the cortical network around a high-efficiency backbone with constant global efficiency and optimal local efficiency behavior is also captured well by the EDR (Fig. 5D). These efficiencies are not binary graph measures, but are based on weights (FLNs). By contrast, the CDR fails completely, especially for the local efficiency measure (Fig. 5D).

Optimal Placement

The ability of the weight-distance relations of the $\boldsymbol{G}_{29\times29}$ to predict numerous features of the cortical network underlines the importance of the embedded nature of real-world networks where nodes are located in three-dimensional (3D) Euclidean space and are linked by weighted and directed edges (88). An important aspect of the embedded cortical network is

the spatial layout of cortical areas. Numerous studies have presented evidence that the spatial layout is optimized to minimize total wire length (89–91). A recent study used collated data for 95 areas of the macaque and claimed that optimized component rearrangements based on a simulated annealing algorithm could substantially reduce total wire (92). However, the database used by that study was edge-incomplete and the network density derived from it had a low density. In addition, weights were only classified as being on one of four levels. We adapted evolutionary optimization algorithms and applied them to our database to search for areal placements that minimize total wire length; we found alternative organizations that shorten the binary network by 5%. For the weighted network, the maximum reduction was less than 1% and involved a small number of switches between adjacent areas (Fig. 6) (13). Figure 6A shows a 3D representation of the $\boldsymbol{G}_{29\times29}$ network with areas color coded to indicate regional identity. Figure 6B is an example of shuffled areal positions leading to increased wire length and loss of adjacency of areas originally from the same region. An optimization procedure applied to the randomized network leads to regional clustering similar to that observed in the cortex (Fig. 6C). Further, random networks based on the EDR had significantly shorter wire lengths than CDR-generated networks. These results therefore confirm that wire minimization is a constitutive organizational principle of the cortical network (89–91, 93–99) and suggest that this design constraint is at least partially implemented by the operation of the EDR generating the weight distributions of interareal projections (13).

Concluding Remarks

In summary, the interareal network achieves economy of connectivity and communication efficiency by means of a distribution of weights, spatial organization and a core-periphery structure in the form of a bow tie with a dense core. Interareal connections integrate across the local circuits via dual counter-streams located in the supra- and infragranular layers, which have distinct physiological properties. Further explorations of the impact of the cortical core on the local circuit should improve our understanding of their dynamic interaction.

The broadband connections involving large number of cells that form the global efficiency backbone and that are expected to shape receptive fields in target areas are short range and strongly cluster areas of a given modality. The considerably more numerous long-distance connections are sparse and exhibit high binary specificity; we speculate that these connections serve to promote cortical communication by controlling oscillatory coherence (77) possibly via contraction dynamics (100). During primate evolution the increase in numbers of areas and their spatially restricted broadband connections raises the possibility that increases in brain size would lead to increased isolation of clustered communities (101, 102). We hypothesize that weak long-distance connections appeared during recent evolution and may facilitate cooperation between distant areas. Assuming that a high-density connectivity is a characteristic feature of the interareal cortical graph, long-distance weak links may allow preservation of the connectedness of the cortical network following cortical expansion. Further, long-distance connections allow accommodation of novel information processing, thereby building over evolutionary time upon the existing repertoire of dynamic functions. There are a number of advantages to be gained (see below) by developing a high efficiency central core that we along with others have observed. Long-distance connections particularly for the higher association areas play a special role in forming the cortical core. The high incidence of long-distance projections involving prefrontal areas (11) suggests a particular importance of this cortical region in core-periphery integration, indicating the cortical core as an important component of higher order interareal architectures (103, 104).

Self-organization in cortical development is well established (105). The findings summarized above suggest interesting parallels with other, highly functional, self-organizing information-processing networks. The high density, yet highly specific nature, of $\boldsymbol{G}_{29\times29}$ suggests a heterogeneous, expandable, and cost-efficient information-processing network subject to evolutionary constraints. In particular, we find (i) high connectivity, (ii) high global accessibility, and (iii) large path diversity. Additional evidence supports several further constraints: (iv) a high bisection bandwidth (Fig. 4D); (v) resilience to connectivity failures (global conductance measurements in Fig. 5D show that during sequential removal of the weakest links, a substantial decline in the network's global efficiency is not reached until a density of 24%); and (vi) incremental expandability that allows addition of new areas to the network during evolution, without a substantial wiring overhaul to maintain or improve performance, also supported by optimal placement studies. The global efficiency and the optimal layout of the $G_{29\times29}$ are supportive of (vi). As seen in Fig. 5D, global efficiency stays constant with weak-link removal. Weak links are long-range and might be more prevalent in large brains. Conversely, adding long-range links (during cortical expansion) seems not to affect the global efficiency, much less worsen it (as would be expected in a complete overhaul). In terms of optimal layout, the total wiring in $G_{29\times29}$ [see (13)] is minimal as a consequence of the EDR. It remains minimal following the addition of new areas with strong links to their neighbors and progressively weaker links to distant areas. This corresponds to an optimal spatial arrangement, consistent with incremental expandability. In an interesting parallel, a recent study on efficient, massive data-processing networks shows that for their purposes, random structures with a pronounced core-periphery organization allow incremental growth without sacrificing their high bisection bandwidth and throughput capability (106).

Although primate neocortex shares a number of common features with human-made, large-scale information-processing networks, there are also crucial differences, and so the analogies should not be overextended. One important difference is that in current technological information networks, information (including a destination address) is encoded within the units (packets) that are sent along the edges of the network (packet-switching networks), whereas this does not appear to be the case for the brain. Our results show that spatial location does influence the wiring properties of the brain. Further, in the brain, the location and timing of activity (in the context of other firing activities) represent the message (neural coding), thus linking network activity to the structural properties of the cortical network. In the Internet or World Wide Web, however, it does not matter where the routers are physically in space, because the packets are routed on the basis of network addresses encoded into the packet. This key difference suggests that spatio-temporal network models should hold more promise for brain science than generic, purely graph theoretical models such as the SW model.

Future Perspectives

While the high density of the binary interareal graph is not consistent with a SW architecture at the computational level of a cortical area, the SW concept may nonetheless be relevant at finer spatial scales. For example, the high clustering and short path lengths indicative of SW architecture are suggested by diffusion magnetic resonance imaging (MRI) analysis at a node scale of a few millimeters (about the size of the voxels) (107). Here, the importance of the SW parameters revealed by this approach must be considered with respect to the methodological thresholding imposed by the whole-brain imaging technique. The nonrandom connectivity at the single-cell level raises the issue of SW architecture at this scale (108, 109). The rich variety of cell identities posits a conceptual challenge for the potential of SW network at the single-cell level. Large-scale circuit mapping at the single-cell level is not currently feasible, although innovative approaches might conceivably

provide the appropriate data in mice (110). At the interareal level, our results indicate that the spatially embedded nature of the cortical network determines many of its properties, such as structural and weighted graph characteristics. Could similar weight-distance relations operate for single neurons, thereby suggesting a similar operational logic over different scales? Like interareal connectivity, local connectivity shows an exponential density decay (10), reflecting the decrease in the likelihood of synaptic contact with distance (111). Also, log-normal distributions like that of interareal weights have been observed for the distribution of synaptic strengths of single neurons (109).

The EDR that we describe shows that the spatial constant of interareal density decay accounts for many of the binary and weighted features of the cortical graph, as well as the important design feature of wire minimization. Given the high scalability of mammalian neocortex, accommodating five orders of magnitude range of brain weight (112), we examined the spatial location of cortical areas in the $\boldsymbol{G}_{29\times29}$ subgraph and found that when magnitude of connections is taken into account, it shows an optimal placement of area positions indicating minimization of metabolic expenditure on total wire length, also well predicted by the EDR. Given these results it will be instructive to explore the weight-distance relations in different species to determine how the decay parameter λ changes with brain size. This may provide insights into a common rule governing scaling properties of the brain and also allow improved extrapolation of our understanding of the connectivity of the macaque brain obtained using invasive techniques to the larger and less directly accessible human brain.

A core-periphery structure has been observed in other self-organized information-processing architectures, both human-made such as the World Wide Web (113) and the Internet (114, 115), and in biological networks, such as in metabolism (116, 117), the immune system (118), and cell signaling (119–121). The resulting bow tie is an evolutionarily favored structure for a wide variety of complex networks (122, 123), expressing the fact that functional or living systems have an input interface, a processing unit, and an output interface. This is because these systems are not in thermodynamic equilibrium and are required to maintain energy and matter flow through the system. While the overall bow-tie structure is common, we have seen that for the brain it emerges through a counterstream organization of the directed links between core and periphery, showing its specific nature when compared to other bow ties in biology or technical networks. However, the full details of this structural organization will only become evident when additional tracer-based anatomical data are incorporated.

Although the interareal connectivity data explored here has revealed interesting features of the cortical network, many additional analyses remain to be done. It will be important to complement the quantification of connectivity by func tional and improved molecular characterization of cortical areas and also of the parent neurons (124–126). A necessary and complementary development will be to use anterograde tracers to examine the laminar integration of interareal connectivity, combining quantification and morphological characterization at the synaptic level (127, 128). Finally, our use of the term “canonical microcircuit” in the sense of a stereotyped circuit constituting a fundamental cortical building block should be tempered by the evidence for large regional differences in cell densities and dendritic arbor sizes (129, 130). While it is generally accepted that the local circuit exhibits cell-specific connectivity across the cortex (thereby conforming to a canonical circuit) and likewise that there are consistent input-output patterns across the different areas (131), there is nevertheless only a single quantitative interlaminar connectivity map, namely, for cat area 17 (132). The concept of the canonical microcircuit provides a coherent framework for thinking about neocortical function, and evidence of variations of local connectivity point to the need to establish additional quantitative

interlaminar maps. Dynamic models built on existing quantitative interlaminar maps (132, 133) give realistic dynamics (134). Extending this type of modeling to include interareal relations becomes a reasonable next step.

Acknowledgments

We acknowledge C. Lamy and P. Misery for histology and M. A. Gariel for data analysis. This work was supported by FP6-2005 IST-1583 (H.K.); FP7-2007 ICT-216593 (H.K.); ANR-11-BSV4-501 (H.K.); LabEx CORTEX (ANR-11-LABX-0042) (H.K.); PN-II-RU-TE-2011-3-0121, FP7-PEOPLE-2011-IIF-299915 (M.E.-R.); National Institute of Mental Health grant R01 MH60974 (D.C.V.E.); Notre Dame's Interdisciplinary Center for Network Science and Applications (iCeNSA) funds; and, in part, by grant FA9550-12-1-0405 from the U.S. Air Force Office of Scientific Research and Defense Advanced Research Projects Agency (Z.T.).

References and Notes

1. Bressler SL, Menon V. Large-scale brain networks in cognition: Emerging methods and principles. Trends Cogn. Sci. 2010; 14:277–290. doi: 10.1016/j.tics.2010.04.004; pmid: 20493761. [PubMed: 20493761]
2. Mountcastle VB. The columnar organization of the neocortex. Brain. 1997; 120:701–722. doi: 10.1093/brain/120.4.701; pmid: 9153131. [PubMed: 9153131]
3. Rosa MG, Tweedale R. Brain maps, great and small: Lessons from comparative studies of primate visual cortical organization. Philos. Trans. R. Soc. Lond. B Biol. Sci. 2005; 360:665–691. doi: 10.1098/rstb.2005.1626; pmid: 15937007. [PubMed: 15937007]
4. Zeki S. The Ferrier Lecture, The Ferrier Lecture 1995 behind the seen: The functional specialization of the brain in space and time. Philos. Trans. R. Soc. Lond. B Biol. Sci. 2005; 360:1145–1183. doi: 10.1098/rstb.2005.1666; pmid: 16147515. [PubMed: 16147515]
5. Schüz, A.; Miller, M. Cortical Areas: Unity and Diversity. Taylor and Francis; London: 2002.
6. Van Essen DC, Glasser MF, Dierker DL, Harwell J. Cortical parcellations of the macaque monkey analyzed on surface-based atlases. Cereb. Cortex. 2012; 22:2227–2240. doi: 10.1093/cercor/bhr290; pmid: 22052704. [PubMed: 22052704]
7. Bressler SL. Inferential constraint sets in the organization of visual expectation. Neuroinformatics. 2004; 2:227–238. doi: 10.1385/NI:2:2:227; pmid: 15319518. [PubMed: 15319518]
8. Markov NT, et al. A weighted and directed interareal connectivity matrix for macaque cerebral cortex. Cereb. Cortex. 2012 doi: 10.1093/cercor/bhs270; pmid: 23010748.
9. Lanciego JL, Wouterlood FG. A half century of experimental neuroanatomical tracing. J. Chem. Neuroanat. 2011; 42:157–183. doi: 10.1016/j.jchemneu.2011.07.001; pmid: 21782932. [PubMed: 21782932]
10. Markov NT, et al. Weight consistency specifies regularities of macaque cortical networks. Cereb. Cortex. 2011; 21:1254–1272. doi: 10.1093/cercor/bhq201; pmid: 21045004. [PubMed: 21045004]
11. Markov NT, et al. The role of long-range connections on the specificity of the macaque interareal cortical network. Proc. Natl. Acad. Sci. U.S.A. 2013; 110:5187–5192. doi: 10.1073/pnas.1218972110; pmid: 23479610. [PubMed: 23479610]
12. Markov NT, et al. The anatomy of hierarchy: Feedforward and feedback pathways in macaque visual cortex. J. Comp. Neurol. 2013 n/a. doi: 10.1002/cne.23458; pmid: 23983048.
13. Ercsey-Ravasz M, et al. A predictive network model of cerebral cortical connectivity based on a distance rule. Neuron. 2013; 80:184–197. doi: 10.1016/j.neuron.2013.07.036; pmid: 24094111. [PubMed: 24094111]
14. Gilbert CD, Wiesel TN. Morphology and intracortical projections of functionally characterised neurones in the cat visual cortex. Nature. 1979; 280:120–125. doi: 10.1038/280120a0; pmid: 552600. [PubMed: 552600]
15. Douglas RJ, Martin KAC, Whitteridge D. A canonical microcircuit for neocortex. Neural Comput. 1989; 1:480–488. doi: 10.1162/neco.1989.1.4.480.
16. Douglas RJ, Koch C, Mahowald M, Martin KA, Suarez HH. Recurrent excitation in neocortical circuits. Science. 1995; 269:981–985. doi: 10.1126/science.7638624; pmid: 7638624. [PubMed: 7638624]

17. Felleman DJ, Van Essen DC. Distributed hierarchical processing in the primate cerebral cortex. Cereb. Cortex. 1991; 1:1–47. doi: 10.1093/cercor/1.1.1; pmid: 1822724. [PubMed: 1822724]
18. Bastos AM, et al. Canonical microcircuits for predictive coding. Neuron. 2012; 76:695–711. doi: 10.1016/j.neuron.2012.10.038; pmid: 23177956. [PubMed: 23177956]
19. Kaas JH, Hackett TA, Tramo MJ. Auditory processing in primate cerebral cortex. Curr. Opin. Neurobiol. 1999; 9:164–170. [published erratum appears in Curr. Opin. Neurobiol. 9, 500 (1999)]. doi: 10.1016/S0959-4388(99)80022-1; pmid: 10322185. [PubMed: 10322185]
20. Boussaoud D, Ungerleider LG, Desimone R. Pathways for motion analysis: Cortical connections of the medial superior temporal and fundus of the superior temporal visual areas in the macaque. J. Comp. Neurol. 1990; 296:462–495. doi: 10.1002/cne.902960311; pmid: 2358548. [PubMed: 2358548]
21. Shipp S. The importance of being agranular: A comparative account of visual and motor cortex. Philos. Trans. R. Soc. Lond. B Biol. Sci. 2005; 360:797–814. doi: 10.1098/rstb.2005.1630; pmid: 15937013. [PubMed: 15937013]
22. Adams RA, Shipp S, Friston KJ. Predictions not commands: Active inference in the motor system. Brain Struct. Funct. 2013; 218:611–643. doi: 10.1007/s00429-012-0475-5; pmid: 23129312. [PubMed: 23129312]
23. Barbas H. Pattern in the laminar origin of corticocortical connections. J. Comp. Neurol. 1986; 252:415–422. doi: 10.1002/cne.902520310; pmid: 3793985. [PubMed: 3793985]
24. Barbas H, Rempel-Clower N. Cortical structure predicts the pattern of corticocortical connections. Cereb. Cortex. 1997; 7:635–646. doi: 10.1093/cercor/7.7.635; pmid: 9373019. [PubMed: 9373019]
25. Koechlin E, Ody C, Kouneiher F. The architecture of cognitive control in the human prefrontal cortex. Science. 2003; 302:1181–1185. doi: 10.1126/science.1088545; pmid: 14615530. [PubMed: 14615530]
26. O'Reilly RC, Herd SA, Pauli WM. Computational models of cognitive control. Curr. Opin. Neurobiol. 2010; 20:257–261. doi: 10.1016/j.conb.2010.01.008; pmid: 20185294. [PubMed: 20185294]
27. Botvinick MM. Hierarchical models of behavior and prefrontal function. Trends Cogn. Sci. 2008; 12:201–208. doi: 10.1016/j.tics.2008.02.009; pmid: 18420448. [PubMed: 18420448]
28. Bullmore E, Sporns O. The economy of brain network organization. Nat. Rev. Neurosci. 2012; 13:336–349. pmid: 22498897. [PubMed: 22498897]
29. Raichle ME. Two views of brain function. Trends Cogn. Sci. 2010; 14:180–190. doi: 10.1016/j.tics.2010.01.008; pmid: 20206576. [PubMed: 20206576]
30. Newman MEJ. The structure and function of complex networks. SIAM Rev. 2003; 45:167–256. doi: 10.1137/S003614450342480.
31. Watts DJ, Strogatz SH. Collective dynamics of `small-world' networks. Nature. 1998; 393:440–442. doi: 10.1038/30918; pmid: 9623998. [PubMed: 9623998]
32. Tononi G, Sporns O, Edelman GM. A measure for brain complexity: Relating functional segregation and integration in the nervous system. Proc. Natl. Acad. Sci. U.S.A. 1994; 91:5033–5037. doi: 10.1073/pnas.91.11.5033; pmid: 8197179. [PubMed: 8197179]
33. Sporns O, Honey CJ. Small worlds inside big brains. Proc. Natl. Acad. Sci. U.S.A. 2006; 103:19219–19220. doi: 10.1073/pnas.0609523103; pmid: 17159140. [PubMed: 17159140]
34. Honey CJ, Kötter R, Breakspear M, Sporns O. Network structure of cerebral cortex shapes functional connectivity on multiple time scales. Proc. Natl. Acad. Sci. U.S.A. 2007; 104:10240–10245. doi: 10.1073/pnas.0701519104; pmid: 17548818. [PubMed: 17548818]
35. Sporns O, Tononi G, Edelman GM. Theoretical neuroanatomy: Relating anatomical and functional connectivity in graphs and cortical connection matrices. Cereb. Cortex. 2000; 10:127–141. doi: 10.1093/cercor/10.2.127; pmid: 10667981. [PubMed: 10667981]
36. Hilgetag CC, Burns GA, O'Neill MA, Scannell JW, Young MP. Anatomical connectivity defines the organization of clusters of cortical areas in the macaque monkey and the cat. Philos. Trans. R. Soc. Lond. B Biol. Sci. 2000; 355:91–110. doi: 10.1098/rstb.2000.0551; pmid: 10703046. [PubMed: 10703046]

37. Stephan KE, et al. Computational analysis of functional connectivity between areas of primate cerebral cortex. Philos. Trans. R. Soc. Lond. B Biol. Sci. 2000; 355:111–126. doi: 10.1098/rstb.2000.0552; pmid: 10703047. [PubMed: 10703047]
38. Sporns O, Zwi JD. The small world of the cerebral cortex. Neuroinformatics. 2004; 2:145–162. doi: 10.1385/NI:2:2:145; pmid: 15319512. [PubMed: 15319512]
39. Kennedy H, Knoblauch K, Toroczkai Z. Why data coherence and quality is critical for understanding interareal cortical networks. Neuroimage. 2013; 80:37–45. doi: 10.1016/j.neuroimage.2013.04.031; pmid: 23603347. [PubMed: 23603347]
40. Vezoli J, et al. Quantitative analysis of connectivity in the visual cortex: Extracting function from structure. Neuroscientist. 2004; 10:476–482. doi: 10.1177/1073858404268478; pmid: 15359013. [PubMed: 15359013]
41. For criteria for inclusion of injection sites, see Markov *et al.* (8); for discussion of the sensitivity and location of uptake zones of the tracers used, see supplementary information in Markov *et al.* (10); for sampling frequency and detection of weak connections see Vezoli *et al.* (40); for atlases and electronic data files, see www.core-nets.org.
42. Newman, MEJ. Networks: An Introduction. Oxford Univ. Press; Oxford: 2010.
43. Young MP. The organization of neural systems in the primate cerebral cortex. Proc. R. Soc. Lond. B Biol. Sci. 1993; 252:13–18. doi: 10.1098/rspb.1993.0040; pmid: 8389046.
44. Modha DS, Singh R. Network architecture of the long-distance pathways in the macaque brain. Proc. Natl. Acad. Sci. U.S.A. 2010; 107:13485–13490. doi: 10.1073/pnas.1008054107; pmid: 20628011. [PubMed: 20628011]
45. Jouve B, Rosenstiehl P, Imbert M. A mathematical approach to the connectivity between the cortical visual areas of the macaque monkey. Cereb. Cortex. 1998; 8:28–39. doi: 10.1093/cercor/8.1.28; pmid: 9510383. [PubMed: 9510383]
46. Barthélemy M. Spatial networks. Phys. Rep. 2011; 499:1–101. doi: 10.1016/j.physrep.2010.11.002.
47. Rockland KS, Pandya DN. Laminar origins and terminations of cortical connections of the occipital lobe in the rhesus monkey. Brain Res. 1979; 179:3–20. doi: 10.1016/0006-8993(79)90485-2; pmid: 116716. [PubMed: 116716]
48. Van Essen DC, Zeki SM. The topographic organization of rhesus monkey prestriate cortex. J. Physiol. 1978; 277:193–226. pmid: 418173. [PubMed: 418173]
49. Wong-Riley M. Reciprocal connections between striate and prestriate cortex in squirrel monkey as demonstrated by combined peroxidase histochemistry and autoradiography. Brain Res. 1978; 147:159–164. doi: 10.1016/0006-8993(78)90781-3; pmid: 77701. [PubMed: 77701]
50. Kaas JH, Lin CS. Cortical projections of area 18 in owl monkeys. Vision Res. 1977; 17:739–741. doi: 10.1016/S0042-6989(77)80013-8; pmid: 414440. [PubMed: 414440]
51. Tigges J, Spatz WB, Tigges M. Reciprocal point-to-point connections between parastriate and striate cortex in the squirrel monkey (Saimiri). J. Comp. Neurol. 1973; 148:481–489. doi: 10.1002/cne.901480406; pmid: 4350354. [PubMed: 4350354]
52. Maunsell JHR, van Essen DC. The connections of the middle temporal visual area (MT) and their relationship to a cortical hierarchy in the macaque monkey. J. Neurosci. 1983; 3:2563–2586. pmid: 6655500. [PubMed: 6655500]
53. Hilgetag CC, O'Neill MA, Young MP. Indeterminate organization of the visual system. Science. 1996; 271:776–777. doi: 10.1126/science.271.5250.776; pmid: 8628990. [PubMed: 8628990]
54. Barone P, Batardiere A, Knoblauch K, Kennedy H. Laminar distribution of neurons in extrastriate areas projecting to visual areas V1 and V4 correlates with the hierarchical rank and indicates the operation of a distance rule. J. Neurosci. 2000; 20:3263–3281. pmid: 10777791. [PubMed: 10777791]
55. Reid AT, Krumnack A, Wanke E, Kötter R. Optimization of cortical hierarchies with continuous scales and ranges. Neuroimage. 2009; 47:611–617. doi: 10.1016/j.neuroimage.2009.04.061; pmid: 19398021. [PubMed: 19398021]
56. Krumnack A, Reid AT, Wanke E, Bezgin G, Kötter R. Criteria for optimizing cortical hierarchies with continuous ranges. Front. Neuroinform. 2010; 4:7. pmid: 20407634. [PubMed: 20407634]

57. Markov NT, Kennedy H. The importance of being hierarchical. Curr. Opin. Neurobiol. 2013; 23:187–194. doi: 10.1016/j.conb.2012.12.008; pmid: 23339864. [PubMed: 23339864]
58. Clavagnier S, Falchier A, Kennedy H. Long-distance feedback projections to area V1: Implications for multisensory integration, spatial awareness, and visual consciousness. Cogn. Affect. Behav. Neurosci. 2004; 4:117–126. doi: 10.3758/CABN.4.2.117; pmid: 15460918. [PubMed: 15460918]
59. Supèr H, Lamme VA. Strength of figure-ground activity in monkey primary visual cortex predicts saccadic reaction time in a delayed detection task. Cereb. Cortex. 2007; 17:1468–1475. doi: 10.1093/cercor/bhl058; pmid: 16920884. [PubMed: 16920884]
60. Jehee JF, Roelfsema PR, Deco G, Murre JM, Lamme VA. Interactions between higher and lower visual areas improve shape selectivity of higher level neurons-explaining crowding phenomena. Brain Res. 2007; 1157:167–176. doi: 10.1016/j.brainres.2007.03.090; pmid: 17540349. [PubMed: 17540349]
61. Scholte HS, Jolij J, Fahrenfort JJ, Lamme VA. Feedforward and recurrent processing in scene segmentation: Electroencephalography and functional magnetic resonance imaging. J. Cogn. Neurosci. 2008; 20:2097–2109. doi: 10.1162/jocn.2008.20142; pmid: 18416684. [PubMed: 18416684]
62. Chen CM, et al. Functional anatomy and interaction of fast and slow visual pathways in macaque monkeys. Cereb. Cortex. 2007; 17:1561–1569. doi: 10.1093/cercor/bhl067; pmid: 16950866. [PubMed: 16950866]
63. Ekstrom LB, Roelfsema PR, Arsenault JT, Bonmassar G, Vanduffel W. Bottom-up dependent gating of frontal signals in early visual cortex. Science. 2008; 321:414–417. doi: 10.1126/science.1153276; pmid: 18635806. [PubMed: 18635806]
64. Self MW, Kooijmans RN, Supèr H, Lamme VA, Roelfsema PR. Different glutamate receptors convey feedforward and recurrent processing in macaque V1. Proc. Natl. Acad. Sci. U.S.A. 2012; 109:11031–11036. doi: 10.1073/pnas.1119527109; pmid: 22615394. [PubMed: 22615394]
65. Kennedy H, Bullier J. A double-labeling investigation of the afferent connectivity to cortical areas V1 and V2 of the macaque monkey. J. Neurosci. 1985; 5:2815–2830. pmid: 3840201. [PubMed: 3840201]
66. Rockland, KS. Extrastriate Cortex in Primates. Rockland, KS.; Kaas, JH.; Peters, A., editors. Vol. vol. 12. Plenum Press; New York: 1997. p. 243-293.
67. Tigges J, et al. Areal and laminar distribution of neurons interconnecting the central visual cortical areas 17, 18, 19, and MT in squirrel monkey (Saimiri). J. Comp. Neurol. 1981; 202:539–560. doi: 10.1002/cne.902020407; pmid: 7298914. [PubMed: 7298914]
68. Bullier, J. 23 Problems in Systems Neuroscience. van Hemmen, JL.; Sejnowski, TJ., editors. Oxford University Press; USA: 2006. p. 103-132.
69. Lee TS, Mumford D. Hierarchical Bayesian inference in the visual cortex. J. Opt. Soc. Am. A Opt. Image Sci. Vis. 2003; 20:1434–1448. doi: 10.1364/JOSAA.20.001434; pmid: 12868647. [PubMed: 12868647]
70. Friston K. The free-energy principle: A unified brain theory? Nat. Rev. Neurosci. 2010; 11:127–138. doi: 10.1038/nrn2787; pmid: 20068583. [PubMed: 20068583]
71. Buffalo EA, Fries P, Landman R, Buschman TJ, Desimone R. Laminar differences in gamma and alpha coherence in the ventral stream. Proc. Natl. Acad. Sci. U.S.A. 2011; 108:11262–11267. doi: 10.1073/pnas.1011284108; pmid: 21690410. [PubMed: 21690410]
72. Xing D, Yeh CI, Burns S, Shapley RM. Laminar analysis of visually evoked activity in the primary visual cortex. Proc. Natl. Acad. Sci. U.S.A. 2012; 109:13871–13876. doi: 10.1073/pnas.1201478109; pmid: 22872866. [PubMed: 22872866]
73. Gregoriou GG, Gotts SJ, Zhou H, Desimone R. High-frequency, long-range coupling between prefrontal and visual cortex during attention. Science. 2009; 324:1207–1210. doi: 10.1126/science.1171402; pmid: 19478185. [PubMed: 19478185]
74. Bosman CA, et al. Attentional stimulus selection through selective synchronization between monkey visual areas. Neuron. 2012; 75:875–888. doi: 10.1016/j.neuron.2012.06.037; pmid: 22958827. [PubMed: 22958827]

75. Salazar RF, Dotson NM, Bressler SL, Gray CM. Content-specific fronto-parietal synchronization during visual working memory. Science. 2012; 338:1097–1100. doi: 10.1126/science.1224000; pmid: 23118014. [PubMed: 23118014]
76. Wang XJ. Neurophysiological and computational principles of cortical rhythms in cognition. Physiol. Rev. 2010; 90:1195–1268. doi: 10.1152/physrev.00035.2008; pmid: 20664082. [PubMed: 20664082]
77. Fries P. A mechanism for cognitive dynamics: Neuronal communication through neuronal coherence. Trends Cogn. Sci. 2005; 9:474–480. doi: 10.1016/j.tics.2005.08.011; pmid: 16150631. [PubMed: 16150631]
78. Anderson JC, Kennedy H, Martin KA. Pathways of attention: Synaptic relationships of frontal eye field to V4, lateral intraparietal cortex, and area 46 in macaque monkey. J. Neurosci. 2011; 31:10872–10881. doi: 10.1523/JNEUROSCI.0622-11.2011; pmid: 21795539. [PubMed: 21795539]
79. Crick F, Koch C. Constraints on cortical and thalamic projections: The no-strong-loops hypothesis. Nature. 1998; 391:245–250. doi: 10.1038/34584; pmid: 9440687. [PubMed: 9440687]
80. Harriger L, van den Heuvel MP, Sporns O. Rich club organization of macaque cerebral cortex and its role in network communication. PLOS ONE. 2012; 7:e46497. doi: 10.1371/journal.pone.0046497; pmid: 23029538. [PubMed: 23029538]
81. de Reus MA, van den Heuvel MP. Rich club organization and intermodule communication in the cat connectome. J. Neurosci. 2013; 33:12929–12939. doi: 10.1523/JNEUROSCI.1448-13.2013; pmid: 23926249. [PubMed: 23926249]
82. van den Heuvel MP, Kahn RS, Goñi J, Sporns O. High-cost, high-capacity backbone for global brain communication. Proc. Natl. Acad. Sci. U.S.A. 2012; 109:11372–11377. doi: 10.1073/pnas.1203593109; pmid: 22711833. [PubMed: 22711833]
83. Bron C, Kerbosch J. Algorithm 457: Finding all cliques of an undirected graph. Commun. ACM. 1973; 16:575–577. doi: 10.1145/362342.362367.
84. Milo R, et al. Superfamilies of evolved and designed networks. Science. 2004; 303:1538–1542. doi: 10.1126/science.1089167; pmid: 15001784. [PubMed: 15001784]
85. Latora V, Marchiori M. Economic small-world behavior in weighted networks. Eur. Phys. J. B. 2003; 32:249–263. doi: 10.1140/epjb/e2003-00095-5.
86. Vragović I, Louis E, Díaz-Guilera A. Efficiency of informational transfer in regular and complex networks. Phys. Rev. E Stat. Nonlin. Soft Matter Phys. 2005; 71(3 Pt. 2A):036122. doi: 10.1103/PhysRevE.71.036122; pmid: 15903508. [PubMed: 15903508]
87. Kitzbichler MG, Henson RN, Smith ML, Nathan PJ, Bullmore ET. Cognitive effort drives workspace configuration of human brain functional networks. J. Neurosci. 2011; 31:8259–8270. doi: 10.1523/JNEUROSCI.0440-11.2011; pmid: 21632947. [PubMed: 21632947]
88. Boccaletti S, Latora V, Moreno Y, Chavez M, Hwang DU. Complex networks: Structure and dynamics. Phys. Rep. 2006; 424:175–308. doi: 10.1016/j.physrep.2005.10.009.
89. Cherniak C, Mokhtarzada Z, Rodriguez-Esteban R, Changizi K. Global optimization of cerebral cortex layout. Proc. Natl. Acad. Sci. U.S.A. 2004; 101:1081–1086. doi: 10.1073/pnas.0305212101; pmid: 14722353. [PubMed: 14722353]
90. Klyachko VA, Stevens CF. Connectivity optimization and the positioning of cortical areas. Proc. Natl. Acad. Sci. U.S.A. 2003; 100:7937–7941. doi: 10.1073/pnas.0932745100; pmid: 12796510. [PubMed: 12796510]
91. Raj A, Chen YH. The wiring economy principle: Connectivity determines anatomy in the human brain. PLOS ONE. 2011; 6:e14832. doi: 10.1371/journal. pone.0014832; pmid: 21915250. [PubMed: 21915250]
92. Kaiser M, Hilgetag CC. Nonoptimal component placement, but short processing paths, due to long-distance projections in neural systems. PLOS Comput. Biol. 2006; 2:e95. doi: 10.1371/journal. pcbi.0020095; pmid: 16848638. [PubMed: 16848638]
93. Cherniak C. Component placement optimization in the brain. J. Neurosci. 1994; 14:2418–2427. pmid: 8158278. [PubMed: 8158278]
94. Cherniak C. Neural wiring optimization. Prog. Brain Res. 2012; 195:361–371. doi: 10.1016/B978-0-444-53860-4.00017-9; pmid: 22230636. [PubMed: 22230636]

95. Cherniak C, Changizi M, Kang D. Large-scale optimization of neuron arbors. Phys. Rev. E Stat. Phys. Plasmas Fluids Relat. Interdiscip. Topics. 1999; 59(5 Pt. B):6001–6009. doi: 10.1103/PhysRevE.59.6001; pmid: 11969583. [PubMed: 11969583]

96. Chklovskii DB. Optimal sizes of dendritic and axonal arbors in a topographic projection. J. Neurophysiol. 2000; 83:2113–2119. pmid: 10758121. [PubMed: 10758121]

97. Chklovskii DB, Schikorski T, Stevens CF. Wiring optimization in cortical circuits. Neuron. 2002; 34:341–347. doi: 10.1016/S0896-6273(02)00679-7; pmid: 11988166. [PubMed: 11988166]

98. Koulakov AA, Chklovskii DB. Orientation preference patterns in mammalian visual cortex: A wire length minimization approach. Neuron. 2001; 29:519–527. doi: 10.1016/S0896-6273(01)00223-9; pmid: 11239440. [PubMed: 11239440]

99. Rivera-Alba M, et al. Wiring economy and volume exclusion determine neuronal placement in the Drosophila brain. Curr. Biol. 2011; 21:2000–2005. doi: 10.1016/j.cub.2011.10.022; pmid: 22119527. [PubMed: 22119527]

100. Wang W, Slotine JJ. On partial contraction analysis for coupled nonlinear oscillators. Biol. Cybern. 2005; 92:38–53. doi: 10.1007/s00422-004-0527-x; pmid: 15650898. [PubMed: 15650898]

101. Herculano-Houzel S, Mota B, Wong P, Kaas JH. Connectivity-driven white matter scaling and folding in primate cerebral cortex. Proc. Natl. Acad. Sci. U.S.A. 2010; 107:19008–19013. doi: 10.1073/pnas.1012590107; pmid: 20956290. [PubMed: 20956290]

102. Douglas RJ, Martin KA. Behavioral architecture of the cortical sheet. Curr. Biol. 2012; 22:R1033–R1038. doi: 10.1016/j.cub.2012.11.017; pmid: 23257185. [PubMed: 23257185]

103. Man K, Kaplan J, Damasio H, Damasio A. Neural convergence and divergence in the mammalian cerebral cortex: From experimental neuroanatomy to functional neuroimaging. J. Comp. Neurol. 2013 10.1002/cne.23408. doi: 10.1002/cne.23408; pmid: 23840023.

104. Dehaene S, Changeux JP. Experimental and theoretical approaches to conscious processing. Neuron. 2011; 70:200–227. doi: 10.1016/j.neuron.2011.03.018; pmid: 21521609. [PubMed: 21521609]

105. Kennedy H, Dehay C. Self-organization and interareal networks in the primate cortex. Prog. Brain Res. 2012; 195:341–360. doi: 10.1016/B978-0-444-53860-4.00016-7; pmid: 22230635. [PubMed: 22230635]

106. Singla, A.; Hong, C-Y.; Popa, L.; Brighten Godfrey, P. 3rd USENIX Workshop on hot topics in cloud computing (HotCloud). 2011.

107. Hagmann P, et al. Mapping human whole-brain structural networks with diffusion MRI. PLOS ONE. 2007; 2:e597. doi: 10.1371/journal.pone.0000597; pmid: 17611629. [PubMed: 17611629]

108. Yoshimura Y, Dantzker JL, Callaway EM. Excitatory cortical neurons form fine-scale functional networks. Nature. 2005; 433:868–873. doi: 10.1038/nature03252; pmid: 15729343. [PubMed: 15729343]

109. Song S, Sjöström PJ, Reigl M, Nelson S, Chklovskii DB. Highly nonrandom features of synaptic connectivity in local cortical circuits. PLOS Biol. 2005; 3:e68. doi: 10.1371/journal.pbio.0030068; pmid: 15737062. [PubMed: 15737062]

110. Zador AM, et al. Sequencing the connectome. PLOS Biol. 2012; 10:e1001411. doi: 10.1371/journal. pbio.1001411; pmid: 23109909. [PubMed: 23109909]

111. Braitenberg, V.; Schüz, A. Cortex: Statistics and Geometry of Neuronal Connectivity. ed. 2. Springer-Verlag; Berlin Heidelberg New York: 1998.

112. Striedter, GF. Principles of Brain Evolution. Sinauer Associates; Sunderland, MA: 2005.

113. Broder A, et al. Graph structure in the Web. Comput. Netw. 2000; 33:309–320. doi: 10.1016/S1389-1286(00)00083-9.

114. Tauro, SL.; Palmer, C.; Siganos, G.; Faloutsos, M. Global Telecommunications Conference, 2001. GLOBECOM'01. IEEE; San Antonio, TX: IEEE; 2001. p. 1667-1671.

115. Siganos G, Tauro SL, Faloutsos M. Jellyfish: A conceptual model for the as internet topology. J. Commun. Networks. 2006; 8:339–350. doi: 10.1109/JCN.2006.6182774.

116. Ma H, et al. The Edinburgh human metabolic network reconstruction and its functional analysis. Mol. Syst. Biol. 2007; 3:135. doi: 10.1038/msb4100177; pmid: 17882155. [PubMed: 17882155]

117. Ma H, Zeng AP. Reconstruction of metabolic networks from genome data and analysis of their global structure for various organisms. Bioinformatics. 2003; 19:270–277. doi: 10.1093/bioinformatics/19.2.270; pmid: 12538249. [PubMed: 12538249]
118. Natarajan M, Lin KM, Hsueh RC, Sternweis PC, Ranganathan R. A global analysis of cross-talk in a mammalian cellular signalling network. Nat. Cell Biol. 2006; 8:571–580. doi: 10.1038/ncb1418; pmid: 16699502. [PubMed: 16699502]
119. Oda K, Kitano H. A comprehensive map of the toll-like receptor signaling network. Mol. Syst. Biol. 2006; 2 0015 (2006).
120. Oda K, Matsuoka Y, Funahashi A, Kitano H. A comprehensive pathway map of epidermal growth factor receptor signaling. Mol. Syst. Biol. 2005; 1 0010 (2005).
121. Polouliakh N, Nock R, Nielsen F, Kitano H. G-protein coupled receptor signaling architecture of mammalian immune cells. PLOS ONE. 2009; 4:e4189. doi: 10.1371/journal.pone.0004189; pmid: 19142232. [PubMed: 19142232]
122. Csete M, Doyle J. Bow ties, metabolism and disease. Trends Biotechnol. 2004; 22:446–450. doi: 10.1016/j.tibtech.2004.07.007; pmid: 15331224. [PubMed: 15331224]
123. Doyle JC, Csete M. Architecture, constraints, and behavior. Proc. Natl. Acad. Sci. U.S.A. 2011; 108(suppl. 3):15624–15630. doi: 10.1073/pnas.1103557108; pmid: 21788505. [PubMed: 21788505]
124. Yamamori T. Selective gene expression in regions of primate neocortex: Implications for cortical specialization. Prog. Neurobiol. 2011; 94:201–222. doi: 10.1016/j.pneurobio.2011.04.008; pmid: 21621585. [PubMed: 21621585]
125. Hof PR, Morrison JH. Neurofilament protein defines regional patterns of cortical organization in the macaque monkey visual system: A quantitative immunohistochemical analysis. J. Comp. Neurol. 1995; 352:161–186. doi: 10.1002/cne.903520202; pmid: 7721988. [PubMed: 7721988]
126. Bernard A, et al. Transcriptional architecture of the primate neocortex. Neuron. 2012; 73:1083–1099. doi: 10.1016/j.neuron.2012.03.002; pmid: 22445337. [PubMed: 22445337]
127. Wang Q, Sporns O, Burkhalter A. Network analysis of corticocortical connections reveals ventral and dorsal processing streams in mouse visual cortex. J. Neurosci. 2012; 32:4386–4399. doi: 10.1523/JNEUROSCI.6063-11.2012; pmid: 22457489. [PubMed: 22457489]
128. Anderson JC, Binzegger T, Martin KA, Rockland KS. The connection from cortical area V1 to V5: A light and electron microscopic study. J. Neurosci. 1998; 18:10525–10540. pmid: 9852590. [PubMed: 9852590]
129. Collins CE. Variability in neuron densities across the cortical sheet in primates. Brain Behav. Evol. 2011; 78:37–50. doi: 10.1159/000327319; pmid: 21691046. [PubMed: 21691046]
130. Wen Q, Stepanyants A, Elston GN, Grosberg AY, Chklovskii DB. Maximization of the connectivity repertoire as a statistical principle governing the shapes of dendritic arbors. Proc. Natl. Acad. Sci. U.S.A. 2009; 106:12536–12541. doi: 10.1073/pnas.0901530106; pmid: 19622738. [PubMed: 19622738]
131. Douglas RJ, Martin KA. Neuronal circuits of the neocortex. Annu. Rev. Neurosci. 2004; 27:419–451. doi: 10.1146/annurev.neuro.27.070203.144152; pmid: 15217339. [PubMed: 15217339]
132. Binzegger T, Douglas RJ, Martin KA. A quantitative map of the circuit of cat primary visual cortex. J. Neurosci. 2004; 24:8441–8453. doi: 10.1523/JNEUROSCI.1400-04.2004; pmid: 15456817. [PubMed: 15456817]
133. Thomson AM, West DC, Wang Y, Bannister AP. Synaptic connections and small circuits involving excitatory and inhibitory neurons in layers 2–5 of adult rat and cat neocortex: Triple intracellular recordings and biocytin labelling in vitro. Cereb. Cortex. 2002; 12:936–953. doi: 10.1093/cercor/12.9.936; pmid: 12183393. [PubMed: 12183393]
134. Potjans TC, Diesmann M. The cell-type specific cortical microcircuit: Relating structure and activity in a full-scale spiking network model. Cereb. Cortex. 2012 doi: 10.1093/cercor/bhs358; pmid: 23203991.
135. Ullman, S. High-Level Vision. Bradford/MIT Press; Cambridge, MA: 2000.
136. Humphries MD, Gurney K, Prescott TJ. The brainstem reticular formation is a small-world, not scale-free, network. Proc. Biol. Sci. 2006; 273:503–511. doi: 10.1098/rspb.2005.3354; pmid: 16615219. [PubMed: 16615219]

Box 1. Efficiency measures for information transfer in networks

In the simplest approximation, we may interpret the FLN weight f_{ij} of the projection from source area i to target area j as the probability $p_{i\to j}$ that activity in i will induce activity in j. Assuming that these are independent events, the probability of activity in area k induced along the path $i\to j\to k$ will be given by the product of the FLNs: $p_{i\to j\to k} = f_{ij}\cdot f_{jk}$ or $\ln(p_{i\to j\to k}) = \ln(p_{i\to j}) + \ln(p_{j\to k})$. Then, the positive quantity $w_{ij} = -\ln(f_{ij})$ can be interpreted as a measure of resistance for information transfer along the $i\to j$ link, as small FLN (weak links) induce a large resistance and vice versa. Additionally, based on our assumption above, the link resistance is additive along network paths. We define the resistance r_{xy} from an arbitrary node x to an arbitrary node y as the smallest sum of link resistances among all directed paths ω_{xy} from x to y, that is, $r_{xy}=\min_{\omega_{xy}}\sum_{(i,j)\in\omega_{xy}} W_{ij}$. The highest transmission probability path will be the one, ω^*_{xy}, that achieves this minimum (see figure). The global efficiency measure E_g is defined as the average conductance (inverse resistance) between all the possible $N(N-1)$ node pairs, where N is the number of nodes in the network as shown in (A).

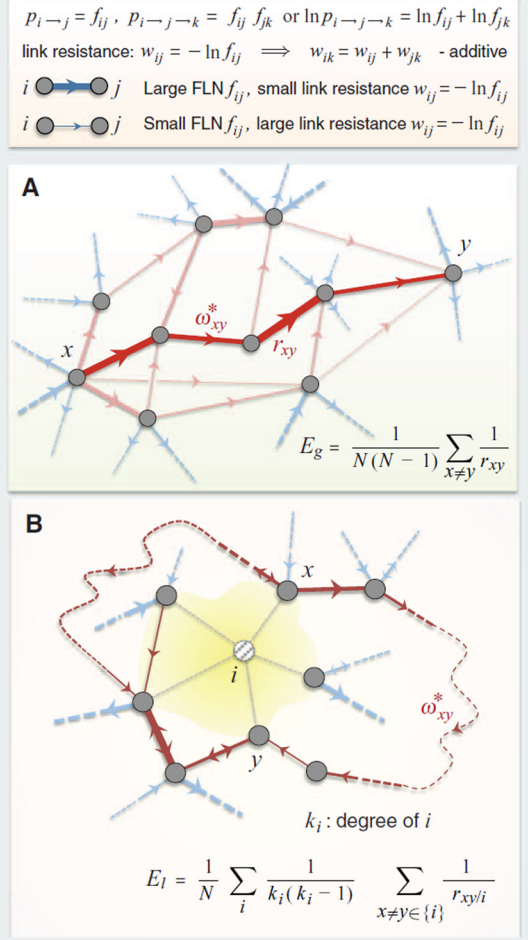

A local efficiency measure E_l is defined in (B): We remove a node i with all its links and then we compute the average of the resistances between all pairs of its neighbors as measured through the rest of the network, and finally, we average these quantities over

all nodes *i*. Thus, E_{l} quantifies the degree to which the satellites of a typical city can communicate via paths that avoid the city (B).

Schematics for efficiency measures

(**A**) Global efficiency and (**B**) local efficiency. The dashed curves are schematic paths through the rest of the network (not shown). Here $\{i\}$ denotes the set of network neighbors of node *i*.

Box 2. Glossary of technical terms

1. **Area:** A region of the cortex with specific cytoarchitecture and associated with a function. **Target area:** An area that received a retrograde tracer injection. **Source area:** An area containing labeled neurons projecting to a target area.
2. **Average path length:** Average value of shortest path lengths between all node pairs in the graph. Length here is measured in hop-counts along directed edges.
3. **Binary specificity:** The degree to which a network or a graph differs in its binary graph theoretical properties from a random graph.
4. **Bisection bandwidth:** The minimum of the number of connections between two, equalsize partitions of the nodes of a graph, taken over all such partitions.
5. **Clustering:** The average of the fraction of connected neighbors of a node (fraction of triangles).
6. **Counterstream:** Refers to the organization principle by which there are streams ascending (supragranular layer) and descending (infragranular layer) the cortical hierarchy (135). Recently, this has been extended to include a dual counterstream organization where an ascending and descending stream is identified in each of the two compartments (12).
7. **Dominating set:** A set of nodes in a graph such that all nodes of the graph have at least one edge with one of their end-nodes in this set.
8. **Edge:** A link or connection between two nodes directed from one to the other, here interareal pathway. There can be at most two directed links, oppositely oriented between any two nodes.
9. **Edge-complete subgraph:** A subgraph that has exactly the same connections between its nodes as the connections between the same nodes in the larger graph that this subgraph is part of.
10. **FLN**: Fraction of labeled neurons: For a given injection (target area *i*) and source area *j*, the FLN is the ratio f_{ij} between the number of labeled neurons in area *j* and the total number of extrinsic (not in *i*) labeled neurons for that injection. We use FLN as a measure of weight (10, 58).
11. $\boldsymbol{G_{nxm}}$ **(sub)graph or matrix:** For every one of the *n* targets (injected areas), it specifies which of the *m* sources project into that target (0 if no projection, 1 if there is a projection). Here, $\boldsymbol{G}_{91\times91}$ denotes the full graph of interareal connections, $\boldsymbol{G}_{29\times91}$ represents the currently known projections from all areas into the injected 29 areas, and $\boldsymbol{G}_{29\times29}$ denotes the subgraph formed by the connections among the target areas only. The latter is edge-complete, i.e., the status of connectivity is fully known within this set of nodes.
12. **Nodes:** Discrete entities represented as points or vertices in graph theory for the purpose of studying the patterns of interactions among them (represented as links or edges). In this case, a node represents a cortical area.
13. **SLN:** The fraction of supragranular labeled neurons is defined for each source area projecting to an injected target area. SLN corresponds to the number of retrogradely labeled neurons located in the supragranular layer divided by the total number of neurons (in infra-and supragranular layers). SLN distinguishes FF and FB pathways and can be used to calculate hierarchical distance (12, 54, 55).

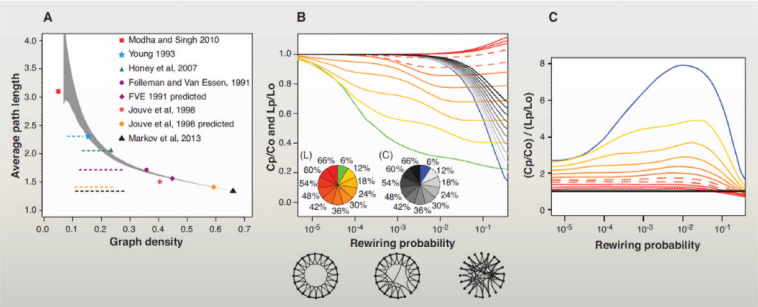

Fig. 1. High density of the cortical graph excludes sparse small-world architecture

(**A**) Comparison of the average shortest path length and density of the $\boldsymbol{G}_{29x29}$ subgraph with the graphs of previous studies. Sequential removal of weak connections causes an increase in the characteristic path-length. Black triangle: $\boldsymbol{G}_{29x29}$; gray area: 95% confidence interval following random removal of connections from $\boldsymbol{G}_{29x29}$. Dotted horizontal lines indicate the 5 to 95% interval with at least one unreachable node (after repeated and graded, random edge removal). The three least dense graphs are near their 5% unreachability levels. Data incompleteness meant that some of the initial networks have unreachable nodes (the latter are removed and not considered here); 14 unreachable nodes are from Modha and Singh (44); 1 unreachable node is from Young (43); and 2 unreachable nodes are from Felleman and Van Essen (17). Modha and Singh 2010: (44); Young 1993: (43); Honey *et al*., 2007: (34); Felleman and Van Essen 1991: (17); Jouve *et al*., 1998: (45); Markov et al., 2012: (8). "Jouve et al., 1998 predicted" indicates values of the graph inferred using the published algorithm (45). (**B**) Effect of density on Watts and Strogatz's formalization of the small world. Clustering and average path-length variations generated by edge rewiring with probability range indicated on the *x* axis applied to regular lattices [of 1000 nodes in a 1D ring as in (31)] of increasingly higher densities. The pie charts show graph density encoded via colors for path length (L) and clustering (C). On the *y* axis, we indicate the average path length ratio (Lp/Lo) and clustering ratio (Cp/Co) of the randomly rewired network, where Lo and Co are the path length (Lo) and clustering (Co) of the regular lattice, respectively. Lp and Cp are the same quantities measured for the network rewired with probability (p). Hence, for each density value indicated in the L and C pie charts, the corresponding Lp/Lo and Cp/Co curves can be identified. Three diagrams below the *x* axis indicate the lattice (left), sparsely rewired (middle), and the randomized (right) networks. (**C**) The small-world coefficient $\frac{Cp/Co}{Lp/Lo}$ (33, 136) corresponding to each lattice rewiring. Color code is the same as in (B). Dashed lines in (B) and (C) indicate 42% and 48% density levels. For electronic data files, see www.core-nets.org.

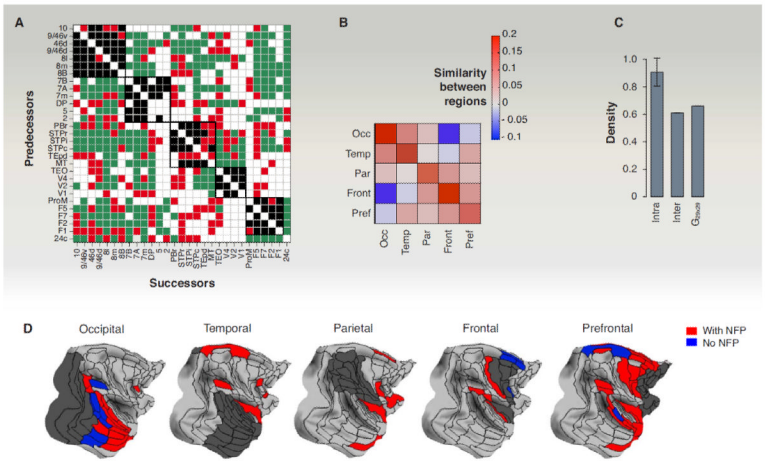

Fig. 2. Binary specificity in the dense network

(A) The ***G****29×29* subgraph adjacency matrix organized so as to illustrate the connectivity within (black squares) and between regions (in green). In red, new-found projections (NFPs). **(B)** Regional in-link similarity of binary connections; positive values indicate positive correlation and negative values indicate anticorrelation between area pairs, within and between regions. The diagonal corresponds to average intraregion similarity; everywhere else is interregion similarity. Occ, occipital region; Temp, temporal region; Par, parietal region; Front, frontal region; Pref, prefrontal. **(C)** Densities of the interregion, intraregion, and ***G****29×29* edge-complete subgraphs. **(D)** Interregion common inputs to one of the five regions (dark gray), including the NFP, increases the number of common inputs. [Panels (B) to (D) adapted from (11)]

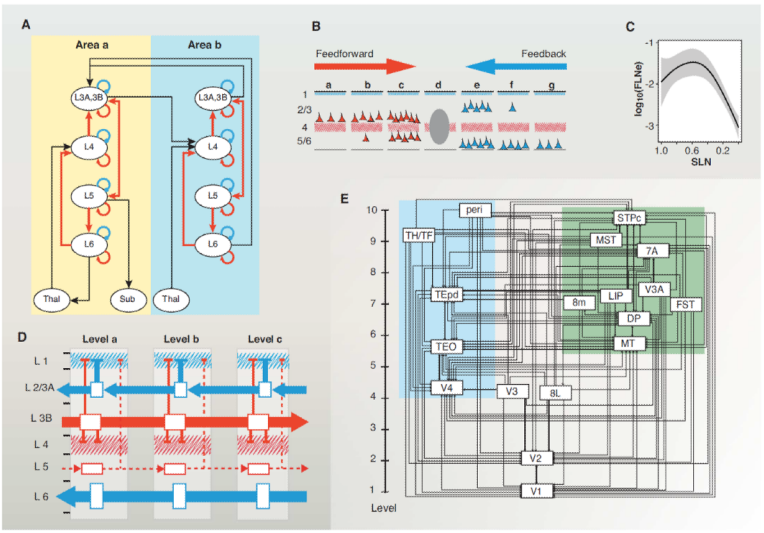

Fig. 3. Cortical hierarchy

(A) Canonical microcircuit [adapted with permission (131)]. **(B)** Cartoon of the laminar distribution of projections to a cortical mid-level area. **(C)** Relationship of SLN and FLN. The strongest pathways are the short-distance lateral connections with an SLN of ~0.5; long-distance FF and particularly FB are substantially weaker. **(D)** Cortical counterstreams. FB and FF are organized in a dual counterstream system localized in supra- and infragranular compartments. In the supragranular compartment, the layer 3B pyramidal cells have long-distance FF axons targeting layer 4 of higher-order areas, while the pyramidal neurons of layer 3A have short-range FB axons targeting the supragranular layers of lower-order areas. In the infragranular compartment, layer 6 has long-distance FB axons that avoid layer 4 and largely target layer 1, whereas layer 5 has short-distance FF axons. Layers 3A and B are the major supragranular output layers and layer 4 is the major input layer for FF projections, and layer 1 the major input layer for FB projections. Apical dendrites of pyramidal cells of layers 3A and 3B and, to a lesser extent, layer 5 reach layer 1, where they can receive FB influences, while some of the basal dendrites of FF layer 3B neurons are located in layer 4. **(E)** A hierarchical organization of the visual cortical areas using SLN as a hierarchical distance measure (12). The projection of area 8L (frontal eye field) to area V4, and from area V4 to area 8L, are both defined by their SLN as FF and therefore form a strong loop (12). (D and E) Color coding: red, FF; blue, FB. [Panel (D) from (12)]. For electronic data files, see www.core-nets.org.

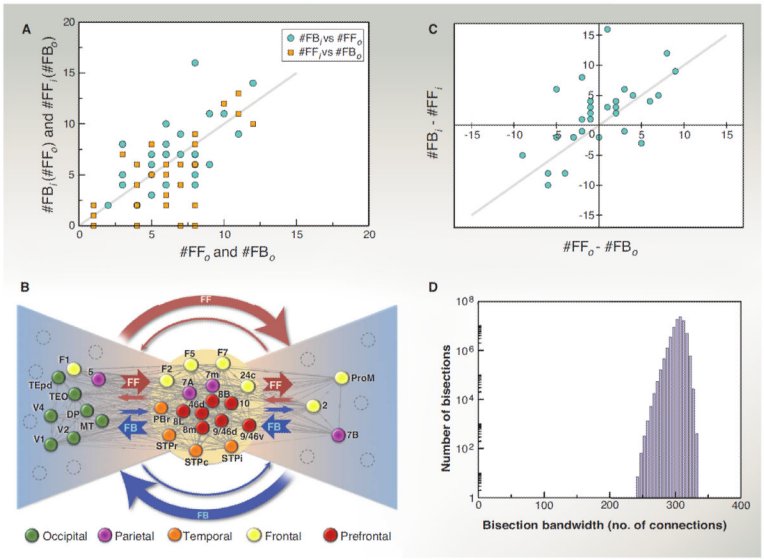

Fig. 4. Bow-tie representation

Links are classified according to their SLN value being below 0.5 (that is, infra dominated, also called FB) or above 0.5 (that is, supra dominated, also called FF) and according to whether they are oriented toward the core ("out" or "o") or from the core ("in" or "i"). This generates a total of four possibilities for link types (*y* is an area from the core, *x* is noncore): (1) *x* projecting to *y* ($x \rightarrow y$) as FF_o (denoted FF_o), (2) $x \rightarrow y$ as FB_o (denoted FB_o), (3) *y* projecting into *x* ($x \leftarrow y$) as FF (or FF_i), and (4) $x \leftarrow y$ as FB (or FB_i). (A) The numbers of link types are correlated over the set of all nodes (both from periphery, P, and core, C); the number of FF links into the core ($\#FF_o$) correlates on average with the number of FB links from the core ($\#FB_i$) and $\#FF_i$ correlates with $\#FB_o$. (B) A bow-tie representation of the ***G****29×29*. The dense core (92%) is shown in the middle. The left and right wings of the tie were obtained based on the FF/FB counterstreams into and from the core and their cumulative effective SLN values; see Table 1 legend for details. The cumulative effective SLN is an average SLN to or from the C for the given connection type, weighted by link strengths. In this way, for every area in the P, we obtain four numbers all between 0 and 1, shown in Table 1, columns F to I. A strong FF into C pairs with a strong FB from C, and vice versa, the connections forming FF/FB counterstreams. Computing two indices of effective SLN strengths in absolute value for the two pairs $|FF_o - 0.5| + |FB_i - 0.5|$ and $|FF_i - 0.5| + |FB_o - 0.5|$ (columns J and K of Table 1), we classify the nodes into one of two groups (L or R) depending on which value is larger. (**C**) The imbalance between the number of FF and FB links from a node to C is mirrored on average by imbalance between the FF and FB connections from C to the same node. (**D**) The edge-complete ***G****29×29* has a very high bisection bandwidth of 242 links, out of 536 total (see Glossary). For electronic data files, see www.core-nets.org.

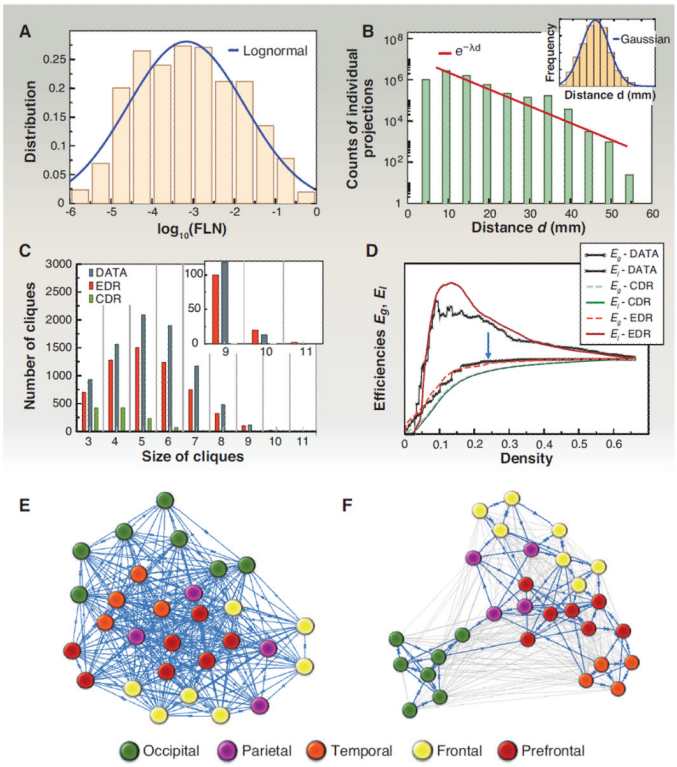

Fig. 5. A spatial network model of the cortex

(A) Distribution of FLN weights and its approximation by a log-normal. (**B**) The number of projections as function of projection distance *d*. (Inset) The distribution of interareal distances through the white matter is well approximated by a Gaussian. (**C**) The distribution of cliques in the ***G****29×29* data network is well captured by the EDR model [see main text and (13)]. (**D**) Global (E_g) and local (E_l) efficiencies (see Box 1) as a function of network density during sequential removal of the weakest link. The EDR model (red) captures both data curves (black) much better than the CDR (green). (**E**) The ***G****29×29* subgraph using a Kamada-Kawaii force-based layout algorithm with all links considered with unit weight. (**F**) Same as (E) but considering the 24% strongest links only [blue arrow in (D)], with FLN weights. In this case, the areas are clustered into functional regions (13). Color code in (E) and (F) refers to regions (see key). For electronic data files, see www.core-nets.org.

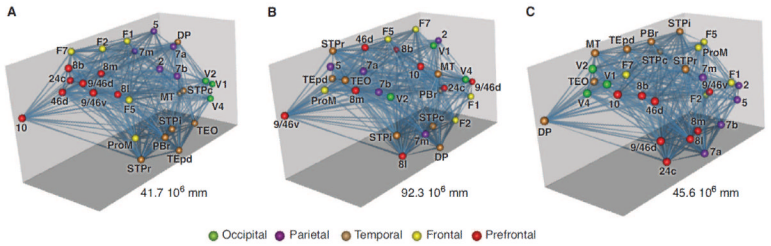

Fig. 6. Spatial positioning of areas and overall wire-length minimization

(A) A 3D representation of ***G****29×29*, nodes positioned at the bary-centers of the corresponding areas identified on brain surface reconstructions (not shown). Edges are visualized as straight lines, but the wire-length calculations for pairs of areas use the axonal trajectory generated as the shortest possible path restricted to the white matter. Color coded for regions (see key). Wire length is the product of the number of neurons involved in the pathway with the estimated pathway length. (**B**) Random repositioning of areas with connectivity preservation leads to wire-length increase. (**C**) An adapted harmony search algorithm reduces the wire length of the starting network in (B). Wire reduction is accompanied by restoration of areal adjacencies. Solutions that fail to reconstruct the initial network exhibit increased wire length with respect to (A). Number in each panel refers to wire lengths.

Table 1

Properties of connections between periphery nodes and the core.

A	B	C	D	E	F	G	H	I	J	K	L
Area	**#FF$_o$**	**#FB$_o$**	**#FF$_i$**	**#FB$_i$**	**FF$_o$−0.5**	**FB$_o$−0.5**	**FF$_i$−0.5**	***FB$_i$−0.5***	**F+|I|**	**|G|+H**	**L/C/R**
2	4	6	3	2	0.136	−0.205	0.063	−0.035	0.171	0.268	R
5	5	6	2	5	0.225	−0.083	0.157	−0.205	0.430	0.240	L
7B	8	3	7	4	0.154	−0.328	0.069	−0.233	0.388	0.397	R-C
DP	10	1	2	11	0.203	−0.268	0.018	−0.158	0.361	0.287	L
F1	6	8	0	8	0.187	−0.253	N/A	−0.073	0.260	0.253	L-C
MT	6	4	4	7	0.384	−0.015	0.174	−0.377	0.760	0.189	L
ProM	2	7	4	2	0.104	−0.199	0.255	−0.145	0.249	0.453	R
TEO	3	4	6	8	0.211	−0.029	0.247	−0.434	0.645	0.276	L
TEpd	3	8	2	8	0.065	−0.336	0.157	−0.104	0.168	0.493	R
V1	3	1	0	4	0.318	−0.500	N/A	−0.442	0.760	0.0	L
V2	8	4	0	5	0.277	−0.260	N/A	−0.394	0.671	0.260	L
V4	8	1	1	6	0.395	−0.500	0.074	−0.463	0.858	0.074	L

All the individual links of an area from P (column A) have been classified into one of four classes. If a link had an SLN > 0.5, it was designated as FF, otherwise as FB. The index "*o*" indicates connections from the node to the core, and the index "*i*" indicates connections from the core into that node. Columns B to E give the number of links of a given type for an area. Columns F to I provide the cumulative effective SLN values (see below) for the four types of connection groups (streams) after subtracting 0.5 from the values. The closer the value to 0.5 (−0.5), the stronger the effective FF (FB) nature of the group of links is. The cumulative effective SLN values were obtained as follows. Let $L_j(x)$ denote the set of nodes in the C that a node x in the P connects with via a link of type j (one of the four types). The effective SLN measure $S_j(x)$ for node x for its connectivity with C, within every link class, weighted by the strength (FLN) of the connections is given by $S_j(x) = (\Sigma y \in L_j(x) s_{xy} f_{xy}) / \Sigma y \in L_j(x) f_{xy}$. Here f_{xy} is the FLN and s_{xy} is the SLN; $s_{xy} f_{xy}$ is thus proportional to the number of supra neurons in that individual (x-y) projection, which is then summed over all connections within that class that node x has with C, normalized by the total strength of the connections within that class. Exploiting the correlations between the streams shown in Fig 4, A to C, we generated in columns J and K two counterstream indices by adding the absolute values of the paired columns. If the outstreams into the C were strong FF (correlated with strong FB from the core), we designated them as L (left wing of the bow tie), otherwise as R (right wing). According to these criteria, TEpd is an outlier; see legend of Fig. 4.